Rotation Drive and Momentum Transport with Electron Cyclotron Heating in Tokamak Plasmas

M. Yoshida, Y. Sakamoto, H. Takenaga, S. Ide, N. Oyama, T. Kobayashi, Y. Kamada, and the JT-60 Team

Japan Atomic Energy Agency, Naka, Ibaraki-ken, 311-0193, Japan

(Received 11 February 2009; published 4 August 2009)

The role of electron cyclotron resonance heating (ECRH) on the toroidal rotation velocity profile has been investigated in the JT-60U tokamak device by separating the effects of the change in momentum transport, the intrinsic rotation by pressure gradient, and the intrinsic rotation by ECRH. It is found that ECRH increases the toroidal momentum diffusivity and the convection velocity. It is also found that ECRH drives the codirection (co) intrinsic rotation inside the EC deposition radius and the counterdirection (ctr) intrinsic rotation outside the EC deposition radius. This ctr rotation starts from the EC deposition radius and propagates to the edge region.

DOI: 10.1103/PhysRevLett.103.065003 PACS numbers: 52.25.Fi, 52.30.−q, 52.55.Fa

It is well known that the toroidal plasma rotation velocity (V_t) and its radial shear play significant roles in improving magnetohydrodynamic (MHD) stability [1–3] and energy confinement in magnetically confined tokamak plasmas [4–6]. There are some discussions on the rotation behavior with electron cyclotron resonance heating (ECRH) [7–10]. For example, the ECRH H-mode plasmas in DIII-D exhibit ctr (the direction antiparallel to the plasma current, or counterdirection) rotation in the core region and co (the direction parallel to the plasma current, or codirection) rotation in the outer region [9]. The toroidal rotation velocity in TCV (tokamak à configuration variable) increases in the codirection by third-harmonic X-mode ECRH together with an increase in the ion temperature (T_i) [10]. Thus an application of ECRH offers a prospect as a rotation control in future devices such as ITER (International Thermonuclear Experimental Reactor), where the auxiliary heating fraction is expected to be small and the rotation driven by the external momentum input may not be dominant [11]. However, the mechanism determining V_t with ECRH has not been well understood due to the complexity of the physics governing the V_t profile. A change in V_t results from multiple processes such as change in momentum transport and drives of intrinsic rotation. The former means that momentum transport varies with ECRH and affects the V_t profile [12,13]. The latter includes the ion thermal pressure gradient (gradP_i)-driven intrinsic rotation [14] in addition to the ECRH-driven intrinsic rotation. Therefore, in order to understand the rotation mechanism with ECRH, it is critically important to investigate these effects individually. In this Letter, the ECRH-driven intrinsic rotation is defined as the change in rotation with ECRH by eliminating the effects of momentum transport and the gradP_i-driven intrinsic rotation. We evaluate the effects of momentum transport and the gradP_i-driven intrinsic rotation by using our original experimental and analytic methods. Then properties of the ECRH-driven intrinsic rotation are extracted. By this approach, we have identified the roles of ECRH on the V_t profile and observed an intriguing intrinsic rotation by ECRH for the first time.

Experiments were conducted in the JT-60U tokamak device [15], where ECRH was injected into neutral beam (NB) heated discharges. JT-60U is equipped with various NBs with different injection geometries: They consist of two codirection tangential beams (co NBs), two counterdirection beams (ctr NBs), and seven near-perpendicular beams (perp NBs). The injection angle of the tangential beams is 36°, and that of the perp NBs is 75° with respect to the magnetic axis. The torque input is varied using a combination of these NBs. The momentum transport coefficients are evaluated by using modulated injection of perp NBs, which enhances ctr rotation locally in the peripheral region of the plasma by the fast ion losses due to the toroidal field ripple [12]. The ECRH power from four gyrotrons of 110 GHz is injected through the antenna mirrors. The mirrors enable steering of the rays in the poloidal cross section, and the EC deposition location is changed by changing the mirror angle. The toroidal injection angle is fixed as 20° from the vertical to the toroidal magnetic field. The V_t and T_i are measured by the Doppler shift and Doppler broadening of the 529.05 nm ($n = 8 \rightarrow 7$) charge exchange (CX) emission from the interaction of fully stripped carbon impurity ions with NB, respectively. In the plasma regime treated in this Letter, the difference between the deuterium V_t and the carbon V_t predicted from the neoclassical theory [16] is negligibly small.

Figure 1(a) shows the radial profiles of V_t for the three cases where ECRH was applied to co, balance (bal), and ctr NB injected positive magnetic shear type-I ELMy (edge localized mode) H-mode plasmas (prior to the EC injection and 0.8 s after the EC injection). In this Letter, the positive and negative signs of V_t designate co and ctr directed rotation, respectively. In the co NB injected plasmas shown by triangles, two units of co tangential NBs and two units of perp NBs were injected. In the ctr NB injected plasmas shown by squares, two units of ctr tangential NBs and two units of perp NBs were injected. In the bal NB injected plasma shown by circles, one unit of co tangential NB, one unit of ctr tangential NB, and two units of perp NBs were injected. All NBs were injected with almost the same

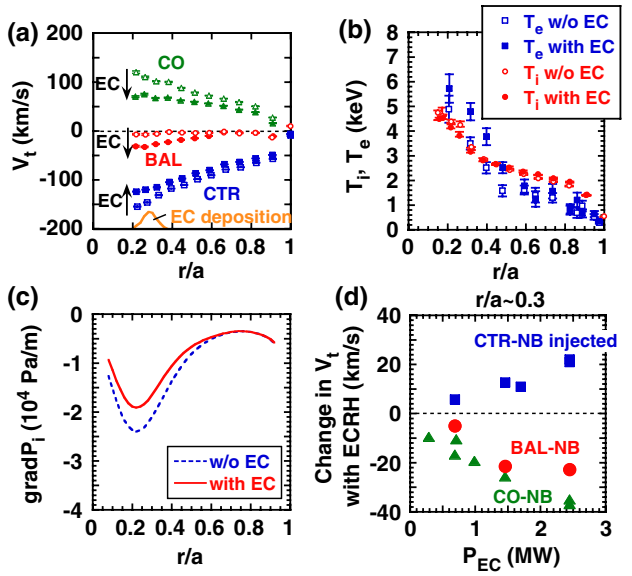

FIG. 1 (color online). (a) The response of the toroidal rotation velocity (V_t) on ECRH in co, bal, and ctr NB injected H-mode plasmas. Solid and open symbols show the data with and without ECRH, respectively. Profiles of (b) the electron temperature (T_e) and the ion temperature (T_i) and (c) the pressure gradient (gradP_i) with and without ECRH for the bal NB injected plasma. (d) The change in V_t at $r/a \sim 0.3$ on the ECRH power.

power of ~2 MW/unit and the same deuterium beam energy of ~85 keV. The main plasma parameters for these plasmas are the plasma current $I_p = 1.0$ MA, the toroidal magnetic field $B_T = 1.8$ T, the major radius $R = 3.4$ m, the plasma minor radius $a = 0.93$ m, the safety factor at the 95% flux surface $q_{95} = 3.7$, the triangularity $\delta = 0.31$, the elongation $\kappa = 1.4$, and the NB heating power $P_{\mathrm{NB}} =$ 5.6–5.8 MW. An electron cyclotron wave of 2.5 MW (2nd harmonic X-mode) was injected at $r/a \sim 0.3$. The absolute values of V_t become smaller in both the co and ctr NB injected plasmas with ECRH. These changes are due mainly to the degradation of momentum confinement with ECRH as discussed later. On the other hand, the change in V_t in the bal NB injected plasma, which is the ctr direction, cannot be explained by the degradation of momentum transport because the external torque input is small as discussed later. The radial profiles of the electron temperature (T_e) measured by the Thomson scattering system and T_i with and without ECRH for the bal NB injected plasma are shown in Fig. 1(b). In the region of $r/a < 0.5$, T_e increases with ECRH; on the other hand, T_i decreases in the region of $r/a < 0.3$. The ion pressure gradient becomes smaller with ECRH at $r/a < 0.5$ as shown in Fig. 1(c). In this Letter, the ion pressure is defined as the sum of the main (deuterium) and impurity (carbon) ion pressures. The increase in ctr rotation for the bal NB injected plasma cannot be explained by the change of the gradP_i-driven intrinsic rotation that has been observed in JT-60U plasmas [14]. These data indicate that ECRH drives the ctr intrinsic rotation. The increase in the T_i pedestal height and the type-I ELM frequency with ECRH were less than 5% and about 20%, respectively. The inversion radius of the sawtooth oscillations was inside of $r/a \sim 0.3$ before and during EC injection. Other MHD modes were not observed. Shown in Fig. 1(d) is a dependence of the change in V_t as a function of the ECRH power (P_{EC}) for each NB injected plasma. The change in V_t increases with increasing ECRH power for both the presence and the absence of external torque.

The change in V_t is discussed from the viewpoint of momentum transport in an ELMy H-mode discharge ($I_p =$ 1.0 MA, $B_T = 3.8$ T, $P_{\mathrm{NB}} = 9.4$ MW, $P_{\mathrm{EC}} = 2.1$ MW with 1st harmonic O-mode, EC deposition $r/a \sim 0.3$). In order to minimize the influence of the change in the momentum transport on the V_t profile, we adopt a discharge with low external torque input (bal NBs). The toroidal momentum diffusivity (χ_ϕ) and the convection velocity (V_{conv}) are determined by the transient momentum transport analysis using perp NBs with the modulated frequency of 2 Hz [13]. It is found that both χ_ϕ and the inward convection velocity ($-V_{\mathrm{conv}}$) increase with ECRH as shown in Figs. 2(a) and 2(b). Figure 2(c) shows the calculated V_t with and without ECRH from the momentum transport equation using χ_ϕ, V_{conv}, the external torque input by NBs, and the boundary condition at $r/a \sim 0.65$ [12,13]. It should be noted that χ_ϕ and V_{conv} vary with ECRH; however, χ_ϕ and V_{conv} do not affect V_t profile in the region $0.3 < r/a < 0.65$ because of the low external torque input. The flatness of the calculated V_t at $r/a < 0.3$ comes from the degradation of momentum confinement under the slight co directed torque input in the core region as shown in Fig. 2(c). The results from Figs. 1(c) and 2 confirm that even though the effects of gradP_i and of momentum transport are taken into account, the ECRH-driven intrinsic rotation is still remarkable: ECRH yields the ctr intrinsic rotation as measured in the bal NB heated plasmas.

In order to identify properties of the ctr intrinsic rotation with ECRH precisely by eliminating the effects of ELMs

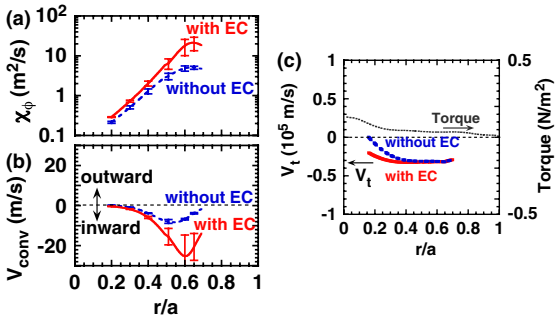

FIG. 2 (color online). Profiles of (a) the toroidal momentum diffusivity (χ_ϕ) and (b) the convection velocity (V_{conv}) with ECRH (solid lines) and without ECRH (dashed lines) in H-mode plasmas. (c) Profiles of the calculated V_t with and without ECRH from the momentum equation with χ_ϕ and V_{conv}. The torque input profile is also shown.

and sawtooth oscillations, response of the V_t profile to ECRH is investigated in positive magnetic shear L-mode plasmas without sawteeth and other MHD modes. Figure 3 shows the time traces of the electron density (n_e), the line averaged electron density ($\bar{n}_e$), the intensity of CX emission (C^{5+}), T_e, V_t, and T_i for a bal NB injected plasma ($I_p = 1.0$ MA, $B_T = 3.8$ T, $R = 3.4$ m, $a = 0.95$ m, $q_{95} = 5.1$, $\delta = 0.33$, $\kappa = 1.4$, and $P_{\mathrm{NB}} = 4.9$ MW), where one unit of co tangential NB, one unit of ctr tangential NB, and two units of perp NBs were injected with almost the same power/unit. Electron cyclotron wave of 2.1 MW was injected from $t = 10$ s (EC deposition $r/a \sim 0.6$). The L-H transition occurs at $t = 10.06$ s shown by the dashed arrow in Fig. 3(a). The electron density and the intensity of CX emission, which is characterizing the carbon ion density (n_c), hardly vary with ECRH as shown in Figs. 3(a) and 3(b). The electron temperature around the EC deposition radius ($r/a \sim 0.6$) increases faster than those at other positions ($t = 9.95$–10.05 s) and saturates at $t \sim 10.08$ s [Fig. 3(c)]. Such evolutions of T_e were observed when the EC deposition radius was varied. The data shown in Fig. 3(c) are T_e at $r/a \sim 0.6$ and 0.84 measured by the multichannel grating polychromator system with a better time resolution than that of the Thomson scattering system. The rotation velocity V_t at $r/a \sim 0.51$ changes in the codirection with ECRH [Fig. 3(d)]. On the other hand, V_t at $r/a \sim 0.65$ changes in the ctr direction [Fig. 3(e)]. Another noteworthy observation is that a rapid change of V_t in the co and ctr directions [shown by black arrows in Figs. 3(d) and 3(e)] occurs, whereas such a rapid change does not appear for n_e and T_i. The ion temperatures at $r/a \sim 0.27$, 0.51, 0.65, and 0.91 remain almost constant as shown in Fig. 3(f). Although the toroidal injection angle of the EC wave is set to a current drive mode, the motional Stark effect signal, which represents the poloidal magnetic field, remains constant in the early phase of EC injection ($t < 10.2$ s).

Figures 4(a) and 4(b) show the V_t profiles at $t = 9.95$ and 10.05 s for the discharge treated in Fig. 3 and the difference in V_t between $t = 9.95$ and 10.05 s, respectively. The profile data of V_t and T_i are averaged for 10 ms in this Letter. The measured V_t in the region $0.3 < r/a < 0.6$ changes in the codirection. On the other hand, V_t in the region $0.6 < r/a < 0.8$ changes in the ctr direction. The difference of V_t for $r/a < 0.3$ cannot be evaluated due to a large measurement scatter. The radial profiles of T_e and T_i are shown in Fig. 4(c). Around the EC deposition of $0.5 < r/a < 0.7$, T_e increases slightly with ECRH. On the other hand, the T_i profile hardly varies. The profiles of T_e, T_i, and V_t in the edge region remain constant. Although gradP_i does not vary with ECRH [Fig. 4(d)], V_t changes in the codirection inside the EC deposition radius as shown in Fig. 4(b). ECRH affects V_t and transport without direct effects on the ion temperature and density. It is also supposed that the change in momentum transport does not vary the V_t profile in the region $0.3 < r/a < 0.65$ from the above-mentioned results [Fig. 2(c)]. In addition, it should

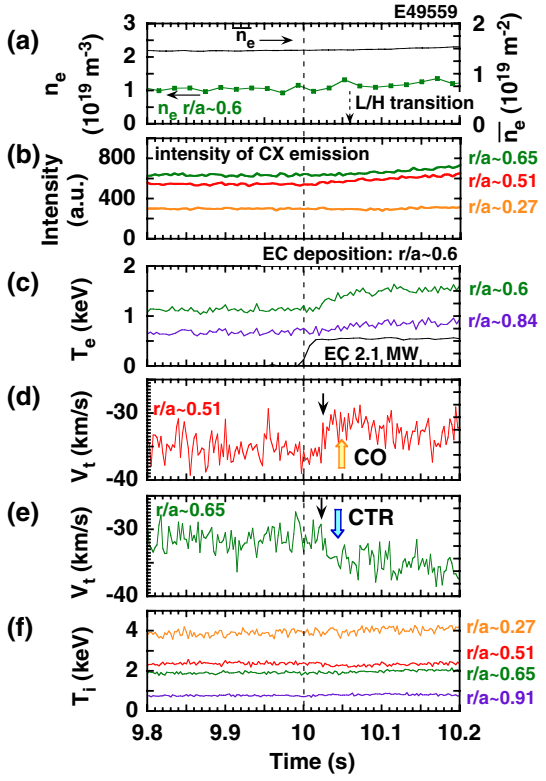

FIG. 3 (color online). Time traces of (a) n_e at $r/a \sim 0.6$ and the line averaged electron density ($\bar{n}_e$), (b) the intensity of CX emission, (c) T_e at $r/a \sim 0.6$ and 0.84, (d) V_t at $r/a \sim 0.51$, and (e) V_t at $r/a \sim 0.65$; the starting time of the change in V_t is shown by black arrows. (f) Waveforms of T_i at $r/a \sim 0.27$, 0.51, 0.65, and 0.91. ECRH is injected from $t = 10$ s.

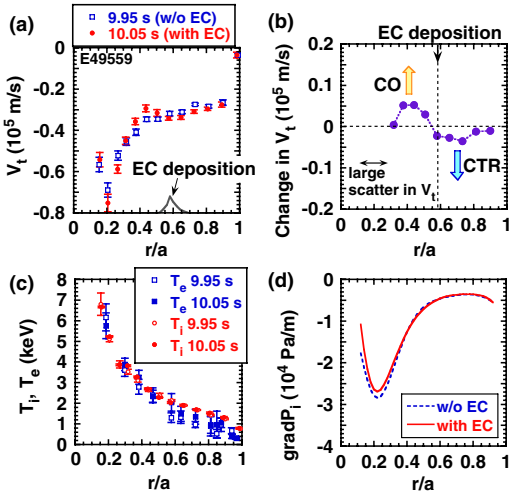

FIG. 4 (color online). (a) Profiles of the measured V_t at $t = 9.95$ (open squares) and 10.05 s (solid circles) in the L-mode phase of the discharge shown in Fig. 3 and EC power deposition. (b) Profiles of the change in V_t with ECRH, i.e., the difference in V_t at $t = 9.95$ and 10.05 s. (c) Profiles of T_e, T_i, and (d) gradP_i, at $t = 9.95$ and 10.05 s.

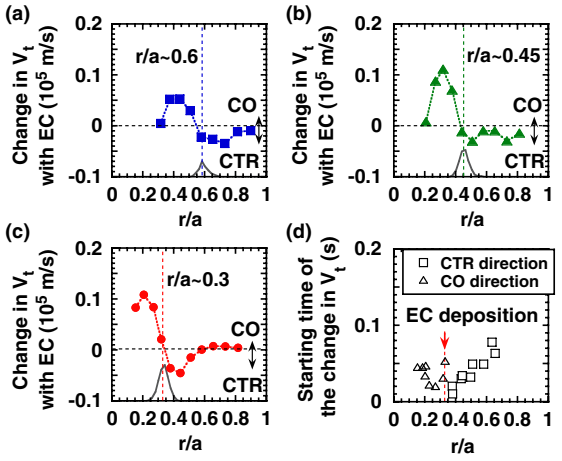

FIG. 5 (color online). Profiles of the change in V_t for each EC deposition: (a) $r/a \sim 0.6$, (b) $r/a \sim 0.45$, and (c) $r/a \sim 0.3$ in the L-mode phase. ECRH power deposition for each case is also shown. (d) Starting time of the change in V_t towards the ctr direction (open squares) and the codirection (open triangles) in the case with $r/a \sim 0.3$ deposition.

be mentioned that the rotation inversion across the EC deposition radius is not due to a reduction of the rotation shear because the rotation shear increases at the EC deposition radius [Fig. 4(a)]. Therefore, the data shown in Fig. 4(b) indicate that ECRH drives the co intrinsic rotation inside the EC deposition radius and the ctr intrinsic rotation outside the EC deposition radius.

As shown in Fig. 4(b), an inversion of the intrinsic rotation is observed around the EC deposition radius of $r/a \sim 0.6$. In order to clarify this interesting phenomenon, an EC deposition scan was performed under an identical discharge condition ($I_p = 1.0$ MA, $B_T = 3.8$ T, $R = 3.4$ m, $a = 0.9$ m, $\delta = 0.33$, $\kappa = 1.4$, and $P_{\mathrm{NB}} = 4.9$ MW). Figures 5(a)–5(c) show the changes in measured V_t with ECRH for each EC deposition: $r/a \sim 0.6$ [the same data shown in Fig. 4(b)], 0.45, and 0.3. The ECRH power deposition profiles for each discharge are also plotted. The ECRH power is 2.1 MW for the $r/a \sim 0.6$ deposition and 2.7 MW for the $r/a \sim 0.3$ and 0.45 depositions. It is clearly observed that the rotation inversion radius varies with the EC deposition radius. In the case with $r/a \sim 0.45$ and 0.3 depositions [Figs. 5(b) and 5(c)], gradP_i becomes smaller with ECRH for $r/a < 0.5$. However, the time scale of the response of V_t is shorter than that of gradP_i. In the $r/a \sim 0.3$ deposition case, a rapid change of V_t in the codirection occurs first ($\sim$0.02–0.04 s after EC injection as discussed later), and then a slow change of co rotation follows inside the EC deposition radius. On the other hand, gradP_i in the core region ($r/a < 0.4$) gradually decreases and reaches a steady state at $\sim$0.07 s after the EC injection. These results conclude that ECRH drives the co intrinsic rotation inside the EC deposition radius and the ctr intrinsic rotation outside the EC deposition radius. There is a possibility that the change in the turbulence with ECRH causes the intrinsic rotation. A theory predicts that the parallel flow is accelerated by turbulence [17]. Another possibility is the enhancement of ctr directed toroidal $E \times B$ velocity by the increase in the negative electric field. When we use the poloidal rotation velocity (V_p) using neoclassical theory to estimate the radial electric field (E_r), E_r becomes more negative with ECRH. We need to evaluate the absolute value of V_p and n_c and measure the turbulence directly to verify the above-mentioned hypotheses. This warrants future work. As mentioned above, the change in V_t in the ctr or co directions starts immediately after the EC injection as shown by black arrows in Figs. 3(d) and 3(e). The starting time of the change in V_t towards the ctr direction in the case with $r/a \sim 0.3$ EC deposition [the same discharge shown in Fig. 5(c)] is plotted against the plasma minor radius by open squares in Fig. 5(d). Also, the starting time of the change in V_t towards the codirection is plotted by open triangles. Although the data of the starting time of the co rotation scatter somewhat, the ctr intrinsic rotation starts from the EC deposition radius and propagates to the edge region.

In conclusion, characteristics of the intrinsic rotation with ECRH have been revealed by separating the effects of the momentum transport and of the pressure gradient driven intrinsic rotation. We have observed the co intrinsic rotation inside the EC deposition radius and the ctr intrinsic rotation outside the EC deposition radius.

[1] D. J. Ward *et al.*, Phys. Plasmas **2**, 1570 (1995).
[2] M. Takechi *et al.*, Phys. Rev. Lett. **98**, 055002 (2007).
[3] H. Reimerdes *et al.*, Phys. Rev. Lett. **98**, 055001 (2007).
[4] Y. Sakamoto *et al.*, Nucl. Fusion **41**, 865 (2001).
[5] E. J. Synakowski *et al.*, Nucl. Fusion **39**, 1733 (1999).
[6] M. R. Wade (DIII-D Team), Nucl. Fusion **47**, S543 (2007).
[7] K. Ida *et al.*, Plasma Phys. Controlled Fusion **44**, 361 (2002).
[8] S. Ide *et al.*, Nucl. Fusion **44**, 87 (2004).
[9] J. S. deGrassie *et al.*, Phys. Plasmas **11**, 4323 (2004).
[10] L. Porte *et al.*, Nucl. Fusion **47**, 952 (2007).
[11] Special issue on Progress in the ITER Physics Basis [Nucl. Fusion **47**, S18 (2007)].
[12] M. Yoshida *et al.*, Plasma Phys. Controlled Fusion **48**, 1673 (2006).
[13] M. Yoshida *et al.*, Nucl. Fusion **47**, 856 (2007).
[14] M. Yoshida *et al.*, Phys. Rev. Lett. **100**, 105002 (2008).
[15] H. Takenaga and the JT-60 Team, Nucl. Fusion **47**, S563 (2007).
[16] Y. B. Kim, P. H. Diamond, and R. J. Groebner, Phys. Fluids B **3**, 2050 (1991).
[17] O. D. Gurcan *et al.*, Phys. Plasmas **14**, 042306 (2007).